RESEARCH ARTICLE

Multitasking in an eye: the unusual organization of the *Thermonectus marmoratus* principal larval eyes allows for far and near vision and might aid in depth perception

Annette Stowasser and Elke K. Buschbeck*

ABSTRACT

Very few visual systems diverge fundamentally from the basic plans of well-studied animal eyes. However, investigating those that do can provide novel insights into visual system function. A particularly unusual system exists in the principal larval eyes of a visually guided aquatic predator, the sunburst diving beetle, *Thermonectus marmoratus* (Coleoptera: Dystiscidae). These eyes are characterized by complex layered distal and proximal retinas. We previously reported that their principal eye E2 has a bifocal lens, and previous behavioral experiments suggested that these larvae have a unilateral range-finding mechanism that may involve their bizarre eye organization. In the present study, we expanded our optical measurements and found that: (1) E1 also has a bifocal lens, (2) E1 is best suited for far vision while E2 is best suited for near vision and (3) throughout their typical hunting range, the positions of focused images shift across specific retinal layers. This anatomical and optical organization in principle could support unilateral range finding. Taken together, our findings outline an unusual visual mechanism that is likely to be essential for the extraordinary hunting ability of these larvae.

INTRODUCTION

Little is known about the function of the eyes (stemmata) of many holometabolous insect larvae, even though they are structurally diverse (Gilbert, 1994). Arguably, among the most complex organized stemmata are the principal eyes of the larvae of the sunburst diving beetle, *Thermonectus marmoratus* Gray 1831 (Coleoptera: Dystiscidae), and it has remained unclear how their bizarre eyes function optically.

Thermonectus marmoratus live in small streams and ponds in the southwest United States (Larson et al., 2009; Morgan, 1992). Their larvae are highly successful visually guided predators that have 12 eyes, six on each side of the head. Four of them (E1 and E2 on each side) are most important for prey capture (Buschbeck et al., 2007) and their organization (Mandapaka et al., 2006) is particularly unusual (Fig. 1). Each of these eyes is characterized by a distinct green-sensitive distal retina (DR) and a UV- and polarization-sensitive proximal retina (PR) (Maksimovic et al., 2011; Stowasser and Buschbeck, 2012). The DR consists of at least 12 tiers of photoreceptor cells that are oriented approximately perpendicular to

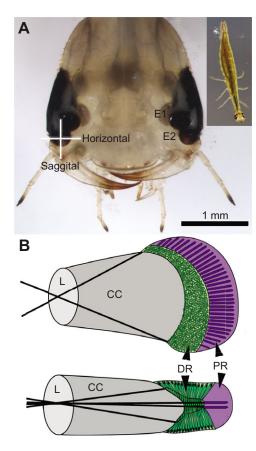Department of Biological Sciences, University of Cincinnati, Cincinnati, OH 45221-0006, USA.

*Author for correspondence (elke.buschbeck@uc.edu)

the light path. The photoreceptors of the PR are organized more conventionally, with their long axis parallel to the light path (Fig. 1B). A previous study has shown that the lens in E2 is bifocal (Stowasser et al., 2010), but whether the second principal eye E1 is also bifocal remains unknown. In addition, it is unclear exactly where on the complex retinal array light is focused, especially in regard to relevant prey distances within their hunting range.

When swimming, larvae approach prey items from a few centimeters (A.S and E.K.B., personal observation), and then strike from a few millimeters distance (in an unpublished study, the average striking distance of third instar larvae was 4.8 mm; S. Werner and E.K.B., unpublished). During the approach, larvae track prey with their principal eyes, which are oriented slightly upwards inside the animal (Mandapaka et al., 2006), but, based on our laboratory observations, are positioned so that these eyes face forward while swimming (Buschbeck et al., 2007). While tracking, the larvae perform scanning movements, which extend the vertically narrow visual fields of these eyes (Buschbeck et al., 2007). Immediately prior to striking, larvae are able to maintain a constant distance to their prey (which occasionally even requires swimming backwards), even if the latter continues to move (Bland et al., 2014; Buschbeck et al., 2007). This behavior, in combination with their ability to maintain typical striking distances when commonly known range-finding mechanisms (Howard, 2012) are severely limited or excluded, suggests that larvae have an unusual mechanism to gauge prey distance (Bland et al., 2014). Specifically, in these experiments on second instars, horizontally moving artificial prey against a homogeneous background confounded potential motion parallax cues. In addition, larvae could not have gauged prey distance simply by the absolute image size, because differently sized prey elicited similar striking distances (means ± s.d.: 4.7±1.3 mm, N=11, and 5.2±1.7 mm, N=8 for small targets and targets double the size, respectively). Finally, typical striking distances remained unchanged even when larvae were unilaterally blinded, demonstrating that bilateral cues were not required. Could larvae use an alternative mechanism, relying on their unusual retinal tiering? Such a mechanism would require that, during all phases of prey approach, reasonably sharp prey images would be projected onto specific, object-distance-dependent retinal layers. Such a mechanism has never been demonstrated in insects, although its possible existence has previously been discussed (Blest et al., 1981; Land, 1969), and it has recently been suggested that differences in defocus between specific retinal layers serve as distance cues in jumping spiders (Nagata et al., 2012), which are also sophisticated visually guided predators (Harland et al., 1999).

Another complication arises from the focal lengths: small eyes typically have short focal lengths and therefore even fairly close objects remain at effective infinity. In contrast, the principal eyes of *T. marmoratus* larvae have long tubes and relatively long focal lengths

Fig. 1. *Thermonectus marmoratus* **third instar larvae.** (A) The entire head with the principal eyes E1 and E2 pointing directly forward. The inset shows an entire larva. (B) Schematic of the principal eyes, showing a horizontal section (top) and a sagittal section (bottom). CC, crystalline cone-like structure; DR, distal retina; L, lens; PR, proximal retina. The black lines indicate the approximate horizontal and vertical visual fields of the retinas. Note that the visual field is wide horizontally but extremely narrow vertically.

(Stowasser et al., 2010). This organization leads to relatively large image sizes and good spatial resolution, which could allow larvae to better resolve prey. However, a long focal length also leads to an enhanced hyperfocal distance (which is the closest distance that remains at effective infinity), so that images from far and near objects necessarily are focused onto different planes. This is especially important if relevant object distances range from effectively infinity to closer than the hyperfocal distance, as is the case for *T. marmoratus*. The need for focusing near and far objects has been discussed for the fairly large lenses of trilobites, which also are thought to have been bifocal, allowing each eye to achieve near and far vision (Egri and Horváth, 2012; Gál et al., 2000a; Gál et al., 2000b).

To determine which optical mechanism could allow *T. marmoratus* larvae to be such successful visually guided predators, it was necessary to establish where images are focused within the eyes. Because chromatic aberration affects image positions, we measured focal lengths with green and UV light. To establish image positions within the eyes, we contrasted the focal lengths of the lenses of the principal eyes from one side of the head with the anatomical eye organization of the contralateral eyes and modeled the image plane locations for close object distances. Based on our findings, we propose that eye- and object-distance-specific positions of focused images are key functional features of the visual system function in *T. marmoratus*.
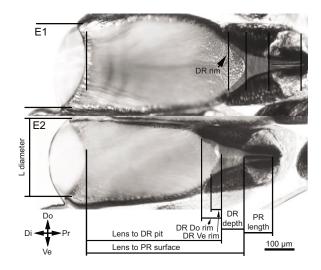
RESULTS

To determine where images are focused within the E1/E2 principal eyes, we needed to: (1) establish precise anatomical measurements of each eye; (2) perform optical measurements that demonstrate where within the eyes images of an object at infinity would be focused; (3) calculate the image's depth of focus; and (4) establish how focused images shift through the retinal layers as objects move closer. Given that the PR is UV-sensitive with a maximal sensitivity to ~375 nm and the DR is green-sensitive with a maximum sensitivity to ~530 nm (Maksimovic et al., 2011), measurements were taken for both wavelengths.

Anatomical measurements: E1 is longer than E2

To establish anatomical parameters and to compare E1 and E2, we took measurements from 19 individuals as illustrated in Fig. 2. Results are summarized in Table 1 and Figs 2 and 4 illustrate the average dimensions of the eyes. All measurements were corrected for shrinkage of 5.9% (±3.1 s.d., N=21), which was assessed from freshly molted third instars (see Materials and methods). Our shrinkage data corresponded well to literature values for comparable tissue preparations. For example, Denef et al. (Denef et al., 1979) found that a 2.5% glutaraldehyde fixation, followed by 1% osmium post-fixation, alcohol dehydration and epoxy resin embedding, led to soft tissue shrinkage of ~6%.

Despite the overall similarity in general morphology between E1 and E2, we found three distinct and significant differences between the two principal eyes. First, the distance between the lens and the pit of both the DR and PR was over 80 µm longer in E1 than in E2 (DR: 82.9±4.7 µm, PR: 82.1±4.3 µm, mean ± s.e., P<0.0007). Despite this substantial difference in overall length, there was no significant difference between the two eyes in regard to the depth of their retinas (see Table 1). Thus, one main difference between E1 and E2 length derives from size differences in the crystalline cone-like structures (which provide spacing between the lenses and retinas). Secondly, the diameter of the lens of E1 was on average 16.3±3.3 µm (P<0.0007) larger than that of E2. Finally, the shape of the rim of the DR is significantly different: in E2, the dorsal rim was on average 29.0±3.0 µm (P<0.0007) longer than its ventral

Fig. 2. Relevant anatomical parameters of E1 and E2. Example sections were morphed to represent average dimensions and were aligned at the back surfaces of the lenses to allow the comparison of the two eyes. Di, distal; Do, dorsal; DR, distal retina; L, lens; PR, proximal retina; Pr, proximal; Ve, ventral.

Table 1. Anatomical measurements of E1 and E2, corrected for 5.9% tissue shrinkage

	E1 (µm)	E2 (µm)
DR Do tip	59±19	66±18
DR Ve tip	57±15	37±11
DR pit	536±26	453±29
PR surface	609±30	527±33
PR length	110±23	98±15
L diameter	278±22	262±19

Values are means ± s.d., N=19.
Do, dorsal; DR, distal retina; L, lens; PR, proximal retina; Ve, ventral.

counterpart, while in E1, there was no significant difference between the dorsal and ventral rim.

Optical measurements: the lenses of both eyes are bifocal, but E1 has longer focal lengths than E2

To characterize the optical properties of both E1 and E2, we measured the focal lengths for each lens under both UV and green light conditions. Table 2 summarizes measurements of the focal lengths (f'; calculated from image magnifications) as well as back focal lengths (f_b; distance between the rear surface of the lens and the location of a focused image of an object at effective infinity). These data confirm that, like E2 (Stowasser et al., 2010), E1 also has a bifocal lens (Fig. 3). In addition, as expected for chromatic aberration, UV light was focused significantly distal to green light in both eyes (E1: Δf_{b1}=29.4±8.0 µm, mean ± s.e., P=0.0037, Δf_{b2}=16.6±7.0 µm, P=0.038, N=12; E2: Δf_{b1}=26.6±5.9 µm, P=0.0012, Δf_{b2}=24.8±4.6 µm, P=0.0003, N=11). Notably, however, we found that for both focal planes, the back focal lengths of E1 were significantly longer than those of E2 (P<0.0001, green: Δf_{b1}=75.4±11.1 µm, Δf_{b2}=108.3±6.9 µm, N=21, UV: Δf_{b1}=79.8±9.5 µm, Δf_{b2}=112.2±11.7 µm, N=8). Moreover, the focal planes in E1 were significantly further apart than in E2 (green: 32.9±9.8 µm, P=0.0031, N=21; UV: 32.4±11.1 µm, P=0.0226, N=8).

Each retina receives its own image

The unusual construction of E1 and E2, the differences in size between them, and their bifocal lenses raise questions of where within each eye the two images are focused. To address this for an object at infinity, we contrasted the back focal lengths, obtained from one side of the head, with anatomical measurements of the contralateral eye (Fig. 4). For green light, we obtained optical and histological data from 13 individuals. This revealed that in both E1 and E2, the first (i.e. the most distal) image fell near the rim of the green-sensitive DR. For the asymmetric DR of E2, this was only the case for the dorsal photoreceptors. Interestingly, despite the overall difference in size between E1 and E2, there was no significant difference in the position of the first image relative to the DR dorsal

tip. In contrast, the second image in E2 was significantly more distal to the image in E1 relative to the surface of the PR (26±9 µm, mean ± s.e., P=0.0134).

Under UV illumination, the second image (i.e. the most proximal) in E1 was focused near the surface of the UV-sensitive PR, providing it with a focused image. In contrast, in E2, the image was positioned distal to the surface of the PR. Based on seven individuals for which we had optical and histological data, we calculated that, relative to the surface of the PR, the second image in E2 was on average 42±17.3 µm (P=0.049) distal to the image in E2 so that the PR of E1 received a focused image of objects at infinity while E2 received a focused image of near objects. To better understand which object distances were still effectively at infinity for these lenses, we calculated the hyperfocal distances. For E1, this distance was 19.8 mm for the first image (measured in green light) and 22.5 mm for the second image (measured in UV light), while for E2, these distances were 14.6 and 17.5 mm, respectively.

To better understand how narrowly an image is focused onto specific retinal layers, we calculated the depth of focus (the range of distances for which an image is in focus along the long/optical axis of the eye) for physical and geometrical optics. With rather conservative assumptions (see Materials and methods), the depth of focus for all relevant object distances was limited by geometrical rather than physical optics (supplementary material Table S1). Our calculations suggest that the depth of focus is restricted to a few retinal layers (Fig. 5).

Next, because the image of a near object (closer than the hyperfocal distance) is focused deeper in the eye than that of an object at infinity, we modeled image positions for relevant object distances (Fig. 5). These findings are particularly important in regards to the green-sensitive DRs, which consist of many retinal tiers in both eyes. Our calculations suggest that, when the object is at infinity, the first images of both bifocal lenses are focused near the top of the DR photoreceptor stacks, while as the object moves closer, focused images pass through the retinal tiers, so that the first few layers are passed when objects move between infinity and ~7 mm. As the object moves even closer, images pass through retinal layers progressively faster, so that in both eyes, objects in typical striking distance are best focused near the pit of the DR, and images have passed through the entire stack at an object distance of 2–3 mm.

Finally, we assessed the magnitude of change in image size that would result from an approaching prey, as this also could potentially be used as a distance cue (Fig. 6). Specifically, we calculated image sizes that would result from two differently sized objects that could, for example, represent prey such as mosquito larvae. Because *T. marmoratus* larvae have a linear retina that is oriented horizontally, we used prey sizes of 0.5 and 0.25 mm, which are realistic values for the widths of these typically vertically oriented prey. Our results suggest that the image size changes drastically when an object is within hunting range of these larvae. For example, based on our E1

Table 2. Back focal length (f_b) and focal length (f') measurements of E1 and E2 for the first and second images in each eye

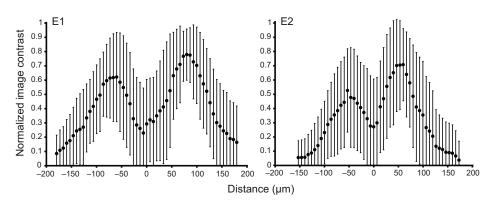|	E1				E2			
	f_b (µm)	N	f' (µm)	N	f_b (µm)	N	f' (µm)	N
Green light								
First	451±51	22	494±57	20	381±36	26	426±48	22
Second	590±25		627±47		485±28		530±32	
UV light								
First	422±47	12	457±62	12	360±29	11	404±39	11
Second	567±23		577±38		463±22		495±37	

Values are means ± s.d.

Fig. 3. Mean (±s.d.) image contrast of E1 and E2 for green light. To pool optical measurements, the rough image contrast of each image series was normalized to a maximum of 1. The image series were aligned to the midpoint between the two focal planes, and the mean was plotted with s.d. Distance (μm) was measured from the midpoint between the two focal planes. The two peaks illustrate the approximate positions of the two best-focused images. For both eyes, the contrast values across all image series at the peaks of the graphs are significantly higher than the contrast values at the midpoint between the two focal planes (*P*≤0.0087, E1: *N*=22, E2: *N*=26).

data of the second focal plane, the smaller object (0.25 mm) would result in the following image sizes: 19.4 μm at 8 mm distance, 42.2 μm at 4 mm distance and 101.5 μm at 2 mm distance. According to these values, the image becomes enlarged by 2.17 times between 8 and 4 mm distance, and 2.41 times between 4 and 2 mm distance. These asymmetries are present because the closer within the near field an object moves towards the lens, the disproportionally more the resulting image moves away from the lens. Accordingly the image is magnified relatively more. Notable here is that the numerical values suggest image sizes that should be easily resolvable by the retinal array of *T. marmoratus*, and that the percentage change in the image size is independent of the absolute size of the object, but instead correlates directly to a specific change in object distance.

DISCUSSION

Arguably, one of the biggest challenges for aquatic predators such as *T. marmoratus* larvae is to resolve and capture prey. This is
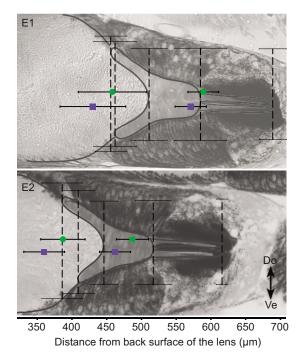

Fig. 4. Comparison between back focal lengths and retinal anatomy. Back focal length measurements for green light are indicated by green circles, and for UV light by blue squares (E1: *N*=10, E2: *N*=11), and illustrate the position of the two best-focused image of an object at infinity. Error bars are ±s.d. Retina schematic and dashed lines illustrate the mean ± s.d. anatomical dimensions (corrected for 5.9% shrinkage). Do, dorsal; Ve, ventral.

particularly difficult in aquatic environments, in which the visibility is often poor because of the scattering of light (Wehner and Labhart, 2006). In addition, aquatic predators are challenged by de-stabilizing water movements that render distance cues, such as motion parallax, ineffective. The extraordinary hunting abilities of *T. marmoratus* larvae indicate that their visual system may have found an elegant way to deal with these challenges. Our results suggest that the organization of their two principal eyes could offer new ways to meet the particular needs of their hunting behavior. Specifically, we found that E1 is well adapted for far vision while E2 better serves near vision, and that, during prey approach, objects tend to be in their near field, allowing for images to be focused onto distinct retinal layers. The latter organization provides a good optical basis for an unusual range-finding mechanism, and may explain recent behavioral findings (Bland et al., 2014) that *T. marmoratus* larvae can successfully gauge distances even when conventional range-finding mechanisms are unavailable.

Together the principal eyes allow for high-resolution as well as near and far vision

One advantage of the tubular eye organization of *T. marmoratus* principal eyes is to provide a relatively high resolving power despite the small size of these animals. This is because these eyes have enhanced focal lengths (~400–600 μm) compared with other insect eyes [e.g. the focal length of the enlarged stemmata of the predatory tiger beetle larvae is ~200 μm (Mizutani and Toh, 1995)]. Generally, twice the focal length results in twice the image magnification and hence the potential for twice the resolution. To take advantage of their long focal lengths, *T. marmoratus* larvae seem to have evolved a mechanism that allows them to have both near and far vision: as image planes shift deeper into the eye for objects that are closer than approximately 2 cm, images are focused on specific retinal layers. Moreover, the systematic differences between E1 and E2 (Fig. 5) explain potential benefits of the presence of two main eyes on each side of the head. The UV-sensitive PR has photoreceptors with relatively typically organized rhabdoms, which presumably can act as light guides (Snyder, 1979). To be maximally excited, a sharp image must be focused on top of the rhabdoms. According to our results, this is the case in the PR of E1 for UV-illuminated objects at infinity, a distance at which the PR of E2 only receives a blurry image. As an object moves into the preferred striking distance (around 3–6 mm), however, the image becomes focused onto the PR of E2, while now the PR of E1 receives a blurry image. Therefore, our data suggest that the UV- and polarization-sensitive PRs are optimized to 'see' well-magnified prey. E1 is optimized to monitor prey during prey approach, and E2 is optimized to monitor prey at striking distance.

Object-distance-dependent dynamics are also apparent in focused green images at the level of the DR (Fig. 5), which in both eyes
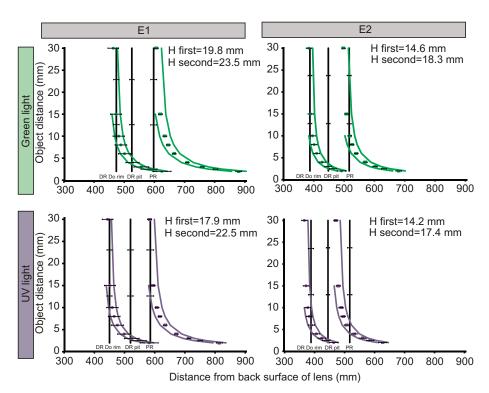
Fig. 5. Image shifts across the retina of objects in the near field. Data points indicate the mean ± s.e. image position, and solid lines indicate the depth of focus. Important anatomical characters (corrected for 5.9% shrinkage) and their s.e. are indicated by vertical lines. DR Do rim, dorsal rim of the distal retina; DR pit, distal retina pit; PR, proximal retina surface. Only preparations for which anatomical and optical data was available were included (E1: green $N=13$ and UV $N=10$; E2: green $N=18$ and UV $N=13$).

consists of at least 12 tiers of shallow cells (Stecher et al., 2010). Within this stack of photoreceptors, cells are expected to be best excited at the level of the best-focused image. Both eyes are organized so that when an object is at infinity, its image is focused near the top of the DR stack. As the object moves closer, the best-focused image moves through the retinal tiers so that, for all relevant object distances, specific layers of the DR receive a focused image while other layers receive consecutively more blurry images. Such a mechanism, however, would require adequate spatial resolution of these receptors, which is the subject of further investigation. Nevertheless, taken together, our optical data suggest that, despite their long focal lengths, these eyes allow the larvae to successfully track prey with both retinas from effective infinity to a few millimeters.

In other visual systems with UV-sensitive photoreceptors, such as crustaceans (Rajkumar et al., 2010), the inner photoreceptors of flies (Hardie, 1985) and jumping spiders (Blest et al., 1981), UV-sensitive cells typically are situated distally to longer-wavelength-sensitive photoreceptors. In jumping spiders, which likewise are sophisticated visual predators (Harland et al., 1999), it has been proposed that this spectral organization corrects for chromatic aberration (Blest et al., 1981; Land, 1969), because shorter wavelengths are focused closer to the lens than longer wavelengths. One might ask, why is the order

of photoreceptors the opposite (Maksimovic et al., 2011) in *T. marmoratus*? Our data suggest that the spectral organization of these eyes, in combination with bifocal lenses, maximizes the distance between the two image planes, which is beneficial, as it minimizes the loss of contrast that results from the interference of the two images.

The eye organization of *T. marmoratus* may support unilateral range finding

Because *T. marmoratus* strike prey from a relatively constant distance (Bland et al., 2014), they must have a suitable mechanism to gauge prey distance. In insects, only a few such mechanisms are well described (Collett and Harkness, 1982). Among the most common and best known is motion parallax, the importance of which has been highlighted in mantids (Kral, 2012), wasps (Zeil, 1993), locusts (Collett, 1978), grasshoppers (Kral, 2009), crickets (Goulet et al., 1981) and bees (Srinivasan et al., 1989). Other somewhat more controversial range-finding mechanisms are based on binocular cues (Kral, 1999; Kral, 2012), such as stereopsis (Rossel, 1983). Finally, insects such as the hoverfly (Collett and Land, 1975) use the absolute image size of objects of known size as a distance cue. However, based on behavioral studies, we recently
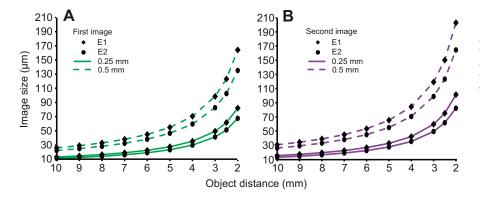

Fig. 6. In the near field, image size dramatically increases as object distance decreases. Illustrated are image sizes of two object sizes that are typical of the widths of prey. (A) The first image size was calculated for green light, because it is projected on the green-sensitive DR. (B) The second image size was calculated for UV light, because this image is primarily projected on the UV-sensitive PR.

discovered that *T. marmoratus* larvae are able to correctly estimate distances, even when none of these mechanisms were available to them (Bland et al., 2014), raising the question of what alternative cues they could be using.

Based on how objects are imaged within the principal eyes of *T. marmoratus* larvae, we identified three alternative possible range-finding cues: (1) the positions of the best-focused images within their retinal tiering, (2) image defocus and (3) the magnitude of the size change of the best-focused image over retinal tiers and/or time. All these mechanisms require that changes in object distance result in substantial image shifts across photoreceptor tiers, and require images to be adequately narrowly focused, as we showed is the case in *T. marmoratus*.

The first possible mechanism (based on the positions of the best-focused images) could function within the DRs of individual eyes. In addition, a focused image is available to the PR of E1 while the prey resides at infinity, and to the PR of E2 at striking distance.

The second mechanism (image defocus) could itself lead to distance information in several ways. First, it could rely on comparing the relative level of defocus between different retinal tiers, as has been proposed for the two proximal tiers of the principal eyes of jumping spiders (Nagata et al., 2012). In *T. marmoratus*, the level of defocus could be assessed across any or all of the many green-sensitive layers of the DR, as well as between the PRs of E1 and E2. Defocus-related distance information could also be obtained from the blurriness of the image at any specific layer, as has been suggested in other systems. For example, in humans, it has been shown that blurriness is an important cue for depth perception (Held et al., 2012; Mather, 1997; Pentland, 1987) that complements stereopsis, and accordingly has been widely applied in computer vision (Chaudhuri and Rajagopalan, 1999). Along those lines, von der Emde et al. (von der Emde et al., 1998) discovered that electrical fish use the blurriness of the electrical image of their surroundings to gain distance information, and Lewis and Maler (Lewis and Maler, 2002) subsequently suggested that using blurriness of sensations in general might be used for gaining more distance information than generally thought. In a very recent paper, defocus-related distance information over time has been suggested to aid in range-finding even in a squid (Chung and Marshall, 2014).

Our third proposed potential mechanism derives distance information from the change in image size of the best-focused image, which is substantial around the typical striking distance of 3–6 mm (Fig. 6). Notably, the percentage change in the image size is independent of the absolute object size, but is instead directly correlated with a specific change in object distance. This cue alone, however, is ambiguous.

Regardless of which of these mechanisms may be most important, it is noteworthy that most of them could be accomplished by responding to activity levels in specific sup-populations of neurons, or by comparing the relative activation of nearby photoreceptors. For this reason it has been proposed that one advantage of defocus-based distance vision is that it requires less complex and more peripheral neurological processing than is required for stereopsis (Held et al., 2012), making it suitable not only for computer vision, but also for animals that have relatively simple nervous systems. This intriguing argument could also be made for the other two mechanisms that we think could contribute to *T. marmoratus*'s ability to accurately assess distances. Which of these mechanisms are implemented thus far remains unclear, and could be further addressed through sophisticated behavioral experiments that, however, need to take these many theoretical possibilities into consideration. However, as so often is the case in nervous systems,

it would not be surprising if several or all of these mechanisms contribute to *T. marmoratus*'s extraordinary ability to catch prey.

MATERIALS AND METHODS
Animals
A population of *T. marmoratus* was maintained in our laboratory throughout the year and larval offspring were reared in isolation on previously frozen bloodworms and live mosquito larvae as previously reported (Stowasser et al., 2010). All data were obtained from third-instar larvae, 1–3 days after ecdysis.

Histology and anatomical measurements
Animals were anesthetized on ice and decapitated, and heads were dissected in 50% insect Ringer's solution (O'Shea and Adams, 1981) as previously reported (Stowasser et al., 2010). To match optics and histology, the lenses of the eyes of one side of the head were measured optically and contrasted to the histology of the other side of the head. The latter was prepared as previously described (Mandapaka et al., 2006). For each individual, the following distances were measured along the long axis of the eye (Fig. 2): (1) the distance between the back surface of the lens and the pit of the DR, (2) the distance between the back surface of the lens and the surface of the PR, (3) the length of the PR and (4) the distance between the pit of the DR and its ventral and dorsal rim. The diameter of the lens was also measured. With the exception of the lens diameter (which was assessed from the section that showed the largest diameter), each individual measurement was based on the average of three to 10 sections from the mid-region of the eye. To correct anatomical measurements for shrinkage, the eye tissue shrinkage during tissue preparation was assessed. To do so, eye tube length of E2 of live, newly molted third instars (before pigmentation of the exoskeleton occluded this eye tube) was compared with histological preparations of the same individuals (processed immediately after photography). All data were tested for normalcy and if not otherwise stated, *P*-values of anatomical comparisons (resulting from two-tailed paired Student's *t*-tests) were corrected for multiple comparisons with Bonferroni correction for seven comparisons.

Optical measurements
As previously described (Stowasser et al., 2010), a microscope was used to observe images formed by the lens. In brief, lenses were mounted with wax between two coverslips so that images were formed between the lenses and the upper coverslip. The space between the coverslips was filled with 50% insect Ringer's solution (O'Shea and Adams, 1981), a concentration that appears to best conserve the lens structure and corresponds well to the osmotic pressure of preliminary hemolymph measurements (A.S., unpublished data). The 'coverslip sandwich' was mounted on a goniometer so that the back surface faced the microscope objective lens. A square-wave grating (0.353 cycles mm^{-1}, USAF 1951 negative test target, Edmund Optics) served as the object and was placed 12.5 cm (effectively at infinity) beneath the stage of a microscope, the condenser of which was removed. The square wave was illuminated with green light (542 nm, half width 47 nm) or UV light (396 nm, half width 78 nm). Photographs were taken at 5 μm intervals from the back surface of each lens to well beyond its two focal planes and evaluated for image contrast using a customized MATLAB program. To establish the positions of the best-focused images, images were cropped to the approximate region of the square wave. For each cropped image, an average grayscale value of each row of the image matrix was computed and plotted (supplementary material Fig. S1A). If plots did not show a wave with three bright bars, the contrast value was set to zero, otherwise the three peak and two trough grayscale values of the wave were found, as illustrated in supplementary material Fig. S1B. Four contrast values were computed from these three maximal (I_{max}) and two minimal (I_{min}) grayscale values (Hecht, 2001), and their average was accepted as a rough estimate of the contrast (C) of the image:

$$C \equiv \frac{I_{max} - I_{min}}{I_{max} + I_{min}}. \quad (1)$$

Generally, the graph of all contrast values across the entire image series showed two peak areas with a trough in between (supplementary material Fig. S1C). For each of the areas surrounding the best-focused images, the

computation was repeated. This time each image was cropped to the portion that only showed the image of the square wave (supplementary material Fig. S1D), and the image with the highest contrast value was accepted as indicative of the true position of the focal plane.

Optical calculations and modeling

First, the tissue that separates the lens was assumed to have a refractive index comparable to that of saline solution. Similar assumptions have been made previously for other eyes (Williams and McIntyre, 1980), and this was further supported by our observation that isolated tissue optically blends in well in saline solution. Because the lenses of these eyes are relatively thick, this optical system was treated as a thick lens system, the focal lengths (f') of which were calculated from image sizes. In each case, first a Gaussian wave was fitted to the average grayscale profile of the best-focused image as illustrated in supplementary material Fig. S1E (Model: gauss3, curve fitting toolbox, MATLAB). The image size was then calculated from the distance between the two outer peaks of the fitted curve and each focal length was calculated following (Hecht, 2001):

$$f' = \frac{y_i}{y_o} S_o ,\qquad (2)$$

where y_i is the image size, y_o is the object size and S_o is the object distance corrected for the refractive index of insect Ringer's solution (1.33) (Hecht, 2001). Additionally, each back focal length (f_b), measured from the back surface of each lens, was calculated from the distance between the image frames that showed the best-focused back surface, and the best-focused respective image (corrected with the refractive index of insect Ringer's solution, 1.33). Finally, for each focal plane, the distance between the second principal plane and the back surface (h_2) was calculated from the focal length (f') and the f_b with $h_2=f'-f_b$. All data were tested for normalcy and analyzed with a two-tailed paired Student's t-test.

Image positions within the eye were modeled for near objects, ranging from 5 cm to 2 mm. To do so, first the image distance (S_i) measured from the second principal plane of the lens was calculated as:

$$S_i = \frac{f' S_o}{S_o - f'} ,\qquad (3)$$

and then, for each image plane, image distances (d_i) were calculated with $d_i=S_i-h_2$ (Hecht, 2001).

To account for overall size variations between individuals, as suggested by Toh and Okamura (Toh and Okamura, 2001), the putative image positions relative to each retina were determined for those individuals for which both optical and anatomical data were available.

To better understand how narrowly images are focused, the depth of focus was assessed, which can be determined by physical (Born and Wolf, 1965) or geometrical optics (Collett and Harkness, 1982) (supplementary material Table S1). Calculations were made for relevant object distances and wavelengths of light similar to what was done for jumping spiders (Land, 1969).

Eqn 4, which is based on the Rayleigh limit, determines limits by physical optics:

$$\Delta d_i = \pm \frac{2\lambda}{n\pi} \left(\frac{R}{a} \right)^2 ,\qquad (4)$$

where Δd_i is the depth of focus for an image at distance S_i, λ is the wavelength of the light (green: λ=540 nm, UV: λ=396 nm), n is the refractive index of the medium behind the lens (n=1.33), R is the radius of the wave front that converges at the optimal image plane, and a is the radius of the exit aperture (Born and Wolf, 1965; Land, 1969). In the principal eyes of *T. marmoratus*, the exit aperture is the pigment ring that surrounds the lens, so that $R=S_i$, and a is half the lens diameter.

Eqns 5 and 6 calculate the depth of focus according to geometrical optics (Collett and Harkness, 1982) (supplementary material Fig. S2):

$$\Delta d_{if} = -\frac{cS_i}{A+c} ,\qquad (5)$$

$$\Delta d_{ic} = -\frac{cS_i}{A-c} .\qquad (6)$$

The depth of focus was calculated for image distances (S_i) of objects that were closer than the hyperfocal distance $H=Af'/c$. Δd_{if} is the depth of focus for object distances that are further away, and Δd_{ic} is the depth of focus for object distances that are closer. A is the lens diameter and c (7 μm) is the diameter of the maximal allowed blur circle, based on the receptor unit spacing of the DR and PR as measured from frontal sections (A.S., unpublished data).

Finally, we determined whether it was theoretically possible for these animals to obtain substantial information from the change in image size that resulted from changes in object distance. For this, we modeled image sizes of two realistic object sizes (based on laboratory experiences, those are 0.25 and 0.5 mm) for object distances between 1 cm and 2 mm (Hecht, 2001):

$$y_i = \frac{S_i}{S_o} y_o .\qquad (7)$$

References

Bland, K., Revetta, N. P., Stowasser, A. and Buschbeck, E. K. (2014). Unilateral range finding in diving beetle larvae. *J. Exp. Biol.* **217**, 327-330.

Blest, A. D., Hardie, R. C., McIntyre, P. and Williams, D. S. (1981). The spectral sensitivities of identified receptors and the function of retinal tiering in the principal eyes of a jumping spider. *J. Comp. Physiol.* **145**, 227-239.

Born, M. and Wolf, E. (1965). *Principles of Optics.* Oxford, UK: Pergamon Press.

Buschbeck, E. K., Sbita, S. J. and Morgan, R. C. (2007). Scanning behavior by larvae of the predacious diving beetle, *Thermonectus marmoratus* (Coleoptera: Dytiscidae) enlarges visual field prior to prey capture. *J. Comp. Physiol. A* **193**, 973-982.

Chaudhuri, S. and Rajagopalan, A. (1999). *Depth From Defocus: A Real Aperture Imaging Approach.* New York, NY: Springer-Verlag.

Chung, W.-S. and Marshall, J. (2014). Range-finding in squid using retinal deformation and image blur. *Curr. Biol.* **24**, R64-R65.

Collett, T. S. (1978). Peering – a locust behaviour pattern for obtaining motion parallax information. *J. Exp. Biol.* **76**, 237-241.

Collett, T. and Harkness, L. (1982). Depth vision in animals. In *Analysis of Visual Behavior* (ed. D. Ingle, M. A. Goodale and R. J. W. Mansfield), pp. 111-176. Cambridge, MA: MIT Press.

Collett, T. S. and Land, M. F. (1975). Visual control of flight behaviour in the hoverfly *Syritta pipiens* L. *J. Comp. Physiol.* **99**, 1-66.

Denef, J. F., Cordier, A. C., Mesquita, M. and Haumont, S. (1979). The influence of fixation procedure, embedding medium and section thickness on morphometric data in thyroid gland. *Histochemistry* **63**, 163-171.

Egri, Á. and Horváth, G. (2012). Possible optical functions of the central core in lenses of trilobite eyes: spherically corrected monofocality or bifocality. *J. Opt. Soc. Am. A Opt. Image Sci. Vis.* **29**, 1965-1976.

Gál, J., Horváth, G. and Clarkson, E. N. K. (2000a). Reconstruction of the shape and optics of the lenses in the abathochroal-eyed trilobite *Neocobboldia chinlinica. Hist. Biol.* **14**, 193-204.

Gál, J., Horváth, G., Clarkson, E. N. K. and Haiman, O. (2000b). Image formation by bifocal lenses in a trilobite eye? *Vision Res.* **40**, 843-853.

Gilbert, C. (1994). Form and function of stemmata in larvae of holometabolous insects. *Annu. Rev. Entomol.* **39**, 323-349.

Goulet, M., Campan, R. and Lambin, M. (1981). The visual perception of relative distances in the wood-cricket, *Nemobius sylvestris. Physiol. Entomol.* **6**, 357-367.

Hardie, R. C. (1985). Functional organization of the fly retina. In *Progress in Sensory Physiology*, Vol. 5 (ed. H. Autrum, D. Ottoson, E. Perl, R. Schmidt, H. Shimazu and W. Willis), pp. 1-79. Berlin, Germany: Springer-Verlag.

Harland, D. P., Jackson, R. R. and Macnab, A. M. (1999). Distances at which jumping spiders (Araneae: Salticidae) distinguish between prey and conspicific rivals. *J. Zool.* **247**, 357-364.

Hecht, E. (2001). *Optics*, 4th edn. Boston, MA: Addison Wesley.

Held, R. T., Cooper, E. A. and Banks, M. S. (2012). Blur and disparity are complementary cues to depth. *Curr. Biol.* **22**, 426-431.

Howard, I. P. (2012). Visual depth perception in the animal kingdom. In *Perceiving in Depth: Other Mechanisms of Depth Perception,* Vol. 3 (ed. I. P. Howard), pp. 233-239. New York, NY: Oxford University Press.

Kral, K. (1999). Binocular vision and distance estimation. In *The Praying Mantids* (ed. F. R. Prete, H. Wells, P. H. Wells and L. E. Hurd), pp. 114-141. Baltimore, MA: The John Hopkins University Press.

Kral, K. (2009). Comparison of the use of active vision for depth perception in three grasshopper families (Orthoptera: Caelifera). *Ann. Entomol. Soc. Am.* **102**, 339-345.

Kral, K. (2012). The functional significance of mantis peering behaviour. *Eur. J. Entomol.* **109**, 295-301.

Land, M. F. (1969). Structure of the retinae of the principal eyes of jumping spiders (Salticidae: Dendryphantinae) in relation to visual optics. *J. Exp. Biol.* **51**, 443-470.

Larson, D. J., Alarie, Y., Roughley, R. E. and Nilsson, A. N. (2009). *Predaceous Diving Beetles (Coleoptera: Dytiscidae) of the Nearctic Region, with Emphasis on the Fauna of Canada and Alaska*. Ottawa, ON: NRC Research Press.

Lewis, J. E. and Maler, L. (2002). Blurring of the senses: common cues for distance perception in diverse sensory systems. *Neuroscience* **114**, 19-22.

Maksimovic, S., Layne, J. E. and Buschbeck, E. K. (2011). Spectral sensitivity of the principal eyes of sunburst diving beetle, *Thermonectus marmoratus* (Coleoptera: Dytiscidae). *J. Exp. Biol.* **214**, 3524-3531.

Mandapaka, K., Morgan, R. C. and Buschbeck, E. K. (2006). Twenty-eight retinas but only twelve eyes: an anatomical analysis of the larval visual system of the diving beetle *Thermonectus marmoratus* (Coleoptera: Dytiscidae). *J. Comp. Neurol.* **497**, 166-181.

Mather, G. (1997). The use of image blur as a depth cue. *Perception* **26**, 1147-1158.

Mizutani, A. and Toh, Y. (1995). Optical and physiological properties of the larval visual system of the tiger beetle, *Cicindela chinensis. J. Comp. Physiol. A* **177**, 591-599.

Morgan, R. C. (1992). Natural history, captive management and the display of the sunburst diving beetle *Thermonectus marmoratus*. In *Proceedings of the AAZPA Annual Conference* 1992, pp. 457-464. Wheeling, VA: American Association of Zoological Parks and Aquariums.

Nagata, T., Koyanagi, M., Tsukamoto, H., Saeki, S., Isono, K., Shichida, Y., Tokunaga, F., Kinoshita, M., Arikawa, K. and Terakita, A. (2012). Depth perception from image defocus in a jumping spider. *Science* **335**, 469-471.

O'Shea, M. and Adams, M. E. (1981). Pentapeptide (proctolin) associated with an identified neuron. *Science* **213**, 567-569.

Pentland, A. P. (1987). A new sense for depth of field. *IEEE Trans. Pattern Anal. Mach. Intell.* **9**, 523-531.

Rajkumar, P., Rollmann, S. M., Cook, T. A. and Layne, J. E. (2010). Molecular evidence for color discrimination in the Atlantic sand fiddler crab, *Uca pugilator. J. Exp. Biol.* **213**, 4240-4248.

Rossel, S. (1983). Binocular stereopsis in an insect. *Nature* **302**, 821-822.

Snyder, A. W. (1979). Physics of vision in compound eyes. In *Handbood of Sensory Physiology*, Vol. 7-6A (ed. H. Autrum), pp. 225-314. Berlin, Germany: Springer-Verlag.

Srinivasan, M. V., Lehrer, M., Zhang, S. W. and Horridge, G. A. (1989). How honeybees measure their distance from objects of unknown size. *J. Comp. Physiol. A* **165**, 605-613.

Stecher, N., Morgan, R. and Buschbeck, E. (2010). Retinal ultrastructure may mediate polarization sensitivity in larvae of the sunburst diving beetle, *Thermonectus marmoratus* (Coleoptera: Dytiscidae). *Zoomorphology* **129**, 141-152.

Stowasser, A. and Buschbeck, E. K. (2012). Electrophysiological evidence for polarization sensitivity in the camera-type eyes of the aquatic predacious insect larva *Thermonectus marmoratus. J. Exp. Biol.* **215**, 3577-3586.

Stowasser, A., Rapaport, A., Layne, J. E., Morgan, R. C. and Buschbeck, E. K. (2010). Biological bifocal lenses with image separation. *Curr. Biol.* **20**, 1482-1486.

Toh, Y. and Okamura, J.-Y. (2001). Behavioural responses of the tiger beetle larva to moving objects: role of binocular and monocular vision. *J. Exp. Biol.* **204**, 615-625.

von der Emde, G., Schwarz, S., Gomez, L., Budelli, R. and Grant, K. (1998). Electric fish measure distance in the dark. *Nature* **395**, 890-894.

Wehner, R. and Labhart, T. (2006). Polarisation vision. In *Invertebrate Vision* (ed. E. J. Warrant and D.-E. Nilsson), pp. 291-348. Cambridge, MA: Cambridge University Press.

Williams, D. S. and McIntyre, P. (1980). The principal eyes of a jumping spider have a telephoto component. *Nature* **288**, 578-580.

Zeil, J. (1993). Orientation flights of solitary wasps (Cerceris; Sphecidae; Hymenoptera). *J. Comp. Physiol. A* **172**, 189-205.